NTNU – Trondheim
Norwegian University of
Science and Technology

Gravity Wave Refraction in the Atmosphere:

Ray tracing versus Geometric Location from a Single Image

Karoline Nærø

Master of Science in Physics and Mathematics
Submission date: June 2013
Supervisor: Patrick Joseph Espy, IFY

Norwegian University of Science and Technology
Department of Physics

This thesis is dedicated to the people who can spend a day looking at the clouds or a night gazing at the stars. They need no further mention; they know who they are.

Acknowledgements

I would like to extend my utmost gratitude to my advisor Prof. Patrick Espy for his invaluable help and insight. I'm forever indebted to my fellow student and friend Morten Hatlen, who wrote the mapping and sine-fitting Matlab code for his own Masters thesis and let me use it in my work. A special thanks to Teferi Demissie for his generous help with GROGRAT.

I should also mention my fellow student and close friend Stine Hverven, whose special brand of optimism goes surprisingly well with own my innate pessimism, and without whose help my references would have been far less organised.

Summary

This thesis presents two methods of finding the sources of gravity waves observed in the night-time hydroxyl airglow; ray-tracing and geometric localisation by fitting concentric circles onto the curvature of the gravity waves' fronts. The observations were made at Dragvoll, Trondheim during winter season of 2012/2013 using an all-sky camera system with a 45° field of view. Wintertime in Trondheim has proved to be a good place to study gravity waves by OH nightglow imaging. Nearly every clear night, the images that were taken captured evidence of gravity wave activity.

This thesis explores the probable sources of the gravity waves. Possible gravity wave sources in the Trondheim area include weather fronts coming in from the western coast, airflow over the Norwegian mountain ridge and auroral activity. Most of the waves were found to propagate from sources in the mountainous inland region of Norway. Given their locations, it is highly likely that these waves are caused by topographic launching. Simply put, topographic launching is airflow over mountains generating waves that propagate freely away from the source region. This is made even more likely by ruling out other possible sources. There is little convective activity in wintertime Norway, making thunderstorms an unlikely source. The fact that the waves propagated from sources near the tropopause rules out auroral activity as the cause of the observed waves.

The geometric localisation method proved to be successful only for waves whose source was located relatively near the imager site. This is because the field of view is too small to accurately discern the curvature of large circular wavefronts. The results from the ray-tracing and the geometric localisation methods were in disagreement with each other. This would suggest that the wave undergoes diffraction as it propagates upwards in the atmosphere.

Sammendrag

Denne avhandlingen presenterer to metoder for å finne kildene til gravitasjonsbølger observert i hydroksyl-airglow om natten; ray-tracing og geometrisk lokalisering ved tilpasning av konsentriske sirkler til gravitasjonsbølgefrontenes krumning. Observasjonene ble gjort på Dragvoll, Trondheim i løpet av vintersesongen 2012/2013 ved hjelp av et all-sky kamerasystem med 45° synsfelt. Vinteren i Trondheim har vist seg å være et godt sted å studere gravitasjonsbølger i OH-airglow. Bildene fra nesten hver eneste klare natt viste spor etter gravitasjonsbølgeaktivitet.

Denne avhandlingen utforsker de sannsynlige kildene til gravitasjonsbølgene. Mulige gravitasjonsbølgekilder i Trondheimsområdet er værfronter som kommer inn fra vestkysten, luftstrømmen over den norske fjellryggen og nordlysaktivitet. De fleste av bølgene viste seg å forplante seg fra kilder i det fjellrike innlandet. Gitt geografien, er det svært sannsynlig at disse bølgene er forårsaket av topografisk aktivitet, dvs. luft som strømmer over fjellene. Ved å utelukke andre mulige kilder, virker denne forklaringen enda mer sannsynlig. Det er liten konvektiv aktivitet vinterstid i Norge, som i seg selv utelukker tordenvær som bølgekilde. Bølgene forplanter seg fra kilder nær tropopausen, og det gjør at nordlysaktivitet fremstår som en usannsynlig kilde.

Geometrisk lokalisering viste seg å bare være vellykket for bølger hvis kilde lå relativt nært kamerastedet. Dette er fordi synsfeltet er for lite til å nøyaktig kunne skilne krumningen til store sirkulære bølgefronter. Resultatene fra ray-tracing og geometrisk lokalisering stemte ikke overens med hverandre. Dette tyder på at bølgen gjennomgår diffraksjon når den forplanter seg oppover i atmosfæren.

TABLE OF CONTENTS

LIST OF TABLES

LIST OF FIGURES

Abbreviations

MLT	=	Mesosphere/Lower Thermosphere
FWHM	=	Full Width Half Maximum
CCD	=	Charge-Coupled Device
HWM	=	Horizontal Wind Model
MSISE	=	Mass-Spectrometer Incoherent Scatter Extended
UTC	=	Coordinated Universal Time
WKB	= Wentzel–Kramers–Brillouin	

CHAPTER 1

INTRODUCTION

Gravity waves are a type of mechanical waves that are generated at the interface between two fluids or inside a fluid. Gravity/buoyancy acts as the restoring force on the wave motion. Atmospheric gravity waves are generated in the atmosphere, commonly in the lower part of the atmosphere and propagate to higher altitudes. As the density decreases with altitude the amplitude of the wave increase until the wave breaks and deposits its momentum.

A fair amount of gravity waves generated in the lower parts of the atmosphere - generally the troposphere - reach mesospheric heights before they break down and deposit their momentum. Coincidentally, the mesosphere is also home to the airglow layers. The airglow layers are (slightly overlapping) regions in the atmosphere in which light is produced through a series of chemical reactions. Hydroxyl, oxygen and sodium are the most important species in these reactions. The airglow layers extend a few kilometres in the vertical direction. The hydroxyl layer, which peaks at 87 km with a FWHM of $\sim$5-8 km is the focus of this study. The OH night-time airglow - referred to as the OH *nightglow* in this paper - provides an excellent opportunity to observe and analyse the gravity wave activity in the mesosphere. As the waves enter the airglow layer the local conditions are perturbed. As the waves propagate the background density takes on the sinusoidal form of the waves; this can be observed in the OH nightglow images as areas of higher and lower intensity relative to the unperturbed background.

The title of this thesis is:*"Gravity Wave Refraction in the Atmosphere: Ray tracing versus Geometric Location from a Single Image"*. This thesis will focus on gravity wave refraction in the atmosphere. The objective is to locate the source of a gravity wave and compare the methods of ray tracing and geometric location. GROGRAT, a linux based gravity wave tracing programme written in fortran, will be used to map the source regions. The aim is to track the source of the gravity waves observed in the OH nightglow - sometimes referred to as the OH airglow or simply airglow in this paper - using two different

approaches and finally compare the results. The different methods are ray-tracing and geometric localisation. The ray-tracing is performed using GROGRAT, a software developed for the exact purpose of tracing non-hydrostatic gravity waves through a gridded numerical representation of Earth's neutral atmosphere, requiring only simple input parameters on the properties of the gravity wave. The process of geometric localisation is a much more crude approach; as opposed to ray-tracing it does not account for diffraction in the atmosphere or the behaviour of the background wind fields. The geometric localisation is carried out by fitting circles to the curvature of the wavefronts in the OH nightglow images.

This paper gives a brief introduction on the theory of atmospheric gravity waves and the chemistry that produces the OH airglow. Possible sources of atmospheric gravity waves are presented. A brief explanation of ray-tracing is given as well as the theory and the assumptions behind the geometric localisation method. Following this, the methods of the data analysis are explained, and then the results are presented in an orderly fashion and then discussed. The two methods are compared. Finally, findings are summarised in the end.

CHAPTER 2
THEORY

The theoretical foundation for this paper is the hydroxyl chemistry in the MLT and the manner in which hydroxyl emits radiation under the local conditions, and the process of how gravity waves are affecting this. Following up, the generation of gravity waves is explained, along with their behaviour in the atmosphere. Finally, several potential sources of gravity waves are mentioned, along with information about the physical phenomena involved in the process.

2.1 The MLT

This entirety of this section is based on Plane, J.M.C.: Atmospheric chemistry of meteoric metals.[Plane, 2003]

The different layers in the atmosphere are defined by the temperature profile of the atmosphere. The region of interest for this paper is the MLT (mesosphere/lower thermosphere). It stretches from about 75 to 110 km in the atmosphere. It is often used as the boundary region between the atmosphere and space. It is a chaotic place, subject to high-energy solar electro-magnetic radiation and solar winds from above, while wave motion in the form of gravity waves, tidal waves and planetary waves deposit momentum into the MLT from below.

The mesosphere begins at the stratopause, at a height of 50 km. In the mesosphere, the temperature decreases with height from a local temperature maxima in the stratopause to a temperature minima in the mesopause. The mesopause is located at about 85 to 100 km, depending on the season. In the thermosphere, located just above the mesopause, the temperature begins to rise with height, caused by the absorption of X-rays and high-energy UV-radiation. Here, temperatures can reach as much as 1000 K, although temperature is nothing but a kinetic concept at this height, since density and pressure are very low. The low temperature in the mesosphere is due to the fact that most of the solar EUV (extreme

ultra-violet), radiation with wavelengths below 120 nm, is absorbed in the thermosphere, while at the same time the pressure in the mesosphere is too low for any significant amount of O_3 formation through O and O_2 recombination. Furthermore, due to the low pressure of the mesosphere, CO_2 acts as a infrared radiator, contributing directly to the cooling.

The MLT is also coldest in summer, as opposed to the lower parts of the atmosphere which are coldest in winter. The gravity waves, which originate in the troposphere from several causes such as orographic forcing, cumulo-nimbus storms, and cyclonic fronts, propagate upwards, their amplitudes increasing with falling pressure. Much momentum is lost in the stratosphere, but waves with the shorter periods reach the upper mesosphere. The low pressure here leads to a collapse of the wave and momentum, and energy is deposited into the MLT. This extra energy leads to a drag on the zonal winds, resulting in a southward meridional flow (for summer in the northern hemisphere). The upwelling air at high latitudes which feeds this flow is cooled by adiabatic expansion. Temperatures may fall below 120 K; if this region were in thermal equilibrium the temperature would be 220 K. At the opposite, winter hemisphere, the air from the summer pole converges and sinks, warming by adiabatic compression to temperatures approaching 250 K.

The very low pressure in the MLT region has several consequences. For one, it means that the mean free path of the air molecules is very large - at 110 km it approaches 1 m. Bulk motion cannot be sustained and diffusion dominates. As for the chemistry, atomic oxygen is the most important reactive species in the MLT. Atomic oxygen is depleted from the MLT at the rate of O_3 forming from the combination of O and O_2. For low pressures, this reaction is pressure dependent. At above 82 km, the time constant for oxygen removal exceeds 12 hours, meaning that an active radical chemistry lives through the night.

2.2 Tropopause

The tropopause is the atmospheric boundary region between the troposphere and the stratosphere. Its height varies greatly with geographic location; it is lowest in the polar regions and highest around the equator. At latitude above 60°N the tropopause is generally less than 9-10 km above sea level [Geerts and Linacre, 1997].

Deep convection in the Intertropical Convergence Zone, or over mid-latitude continents in summer, will push the tropopause upwards. Thunderstorms mixes the tropospheric air at a moist adiabatic lapse rate, which is generally the same as the dry adiabatic lapse rate in the upper troposphere of about 10 K/km. That is, a 10 K temperature drop results in a deepening of the tropopause by 1 km. Consequently, the tropopause is exceptionally high when the tropopause temperature is particularly low; it can drop below -80°C at times [Geerts and Linacre, 1997].

At the same time, the tropopause is lower in colder regions. Limited convective overturning, which is caused by a negative radiative balance on the surface of the Earth, is responsible for this. Convection is rare in polar regions; here, tropospheric mixing is

mostly caused by frontal systems in which uplift is forced rather than spontaneous [Geerts and Linacre, 1997].

2.3 Critical Layer Filtering

Critical layer filtering occurs when the background wind field in the direction of the wave motion matches the observed phase speed. As this happens, the intrinsic wave frequency is reduced to zero by Doppler shifting, and the wave is absorbed into the background mean flow [Nielsen et al., 2009]. This phenomenon is accountable for many upwards propagating gravity waves originating in the lower part of the atmosphere never making it as far as the mesosphere. This is particularly relevant to this thesis, as GROGRAT is very sensitive to changes in the background field in whether a wave is evanescent or an upwards propagating wave.

2.4 Stratospheric Sudden Warming

Global scale disturbances are created in the troposphere and propagate upwards to the stratosphere, where the waves disrupt the polar night jet by decelerating it through a process of induction through meridional circulation. This leads to the distortion and eventual break-down of the polar vortex. The major features of a stratospheric sudden warming are: (1) the distortion and break-down of the polar vortex, (2) the sudden warming of the polar air, which eventually leads to a reversal of the meridional temperature gradient, and (3) the appearance of circumpolar easterly winds succeeding the weakening and disappearance of the polar night westerly jet. [Matsuno, 1971]

The warming of the polar air is caused by poleward heat-transport of planetary waves. In the presence of such eddy processes, mean upwards motion may be induced by the convergence of the heat flux at higher latitudes and and downward motion at lower latitudes. The mean meridional flow is accompanied by vertical motions and the zonal winds are accelerated. Easterly accelerated zonal winds must occur with warming on the higher latitude side at the leading edge of waves or at a critical surface, if the waves are incident on it. [Matsuno, 1971]

A stratospheric sudden warming can have a significant effect on upwards gravity wave propagation. The weakening of the polar night jet may result in the removal of the barrier it poses to wave propagation in this region[Matsuno, 1971].

In January, a stratospheric sudden warming was observed around Trondheim. It lasted approximately from January 10-20, see figure 2.1. In this time period, very high gravity wave activity was observed in the airglow images, and many of the results used in this thesis are from this time period.

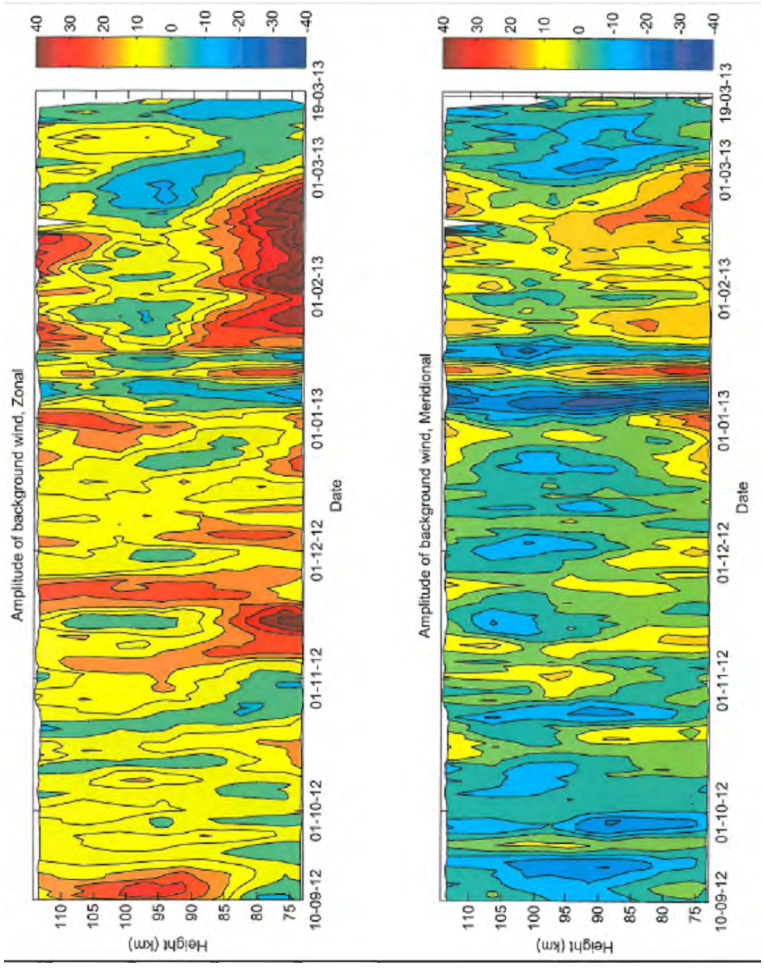

Figure 2.1: Amplitude map of zonal and meridional background winds in the MLT in the winter season 2012/2013 over Trondheim.[R.Hibbins, 2013]

2.5 Relationship between Vertical and Horizontal Wavelengths

By airglow imaging, it is only possible to measure horizontal wavelengths, λ_x. This poses a problems, as the vertical wavelength, λ_z is important for the calculation of the GROGRAT inputs. However, are exist ways of relating the two. [Swenson and Liu, 1998]. In their paper from 1998, Swenson and Liu presented the following relationship between λ_x and λ_z:

$$\lambda_z = \frac{\lambda_x}{\tau_1}\tau_{BV} = C_1\tau_{BV} \tag{2.1}$$

where τ_{BV} and τ_1 is the Brunt Vaisala and intrinsic wave frequency, and C_1 is the intrinsic phase speed.

2.6 Theory of Ray-Tracing

In a medium such as the atmosphere, characteristics such as velocity of propagation, absorption coefficients and reflective and refractive properties may change. Consequently, a wave propagating through the atmosphere will change it course several times. Ray-tracing is a method of calculating the path of a the wave through a such a system. As a wave propagates through such a system the wavefronts may bend, change direction or reflect off a surface. The key principle of ray tracing is to simplify the calculations by transmitting very narrow beams, i.e. rays, though the system.

The key point of ray tracing is the very narrow beams, referred to as *rays* from here on, being used to model the wave. Over a certain distance, generally small compared to the dimensions of the system, the ray is straight. The ray tracer will further the ray over the this distance, and use a local derivative of the medium to calculate the new direction of propagation of the ray. From the endpoint of this ray, another is sent out in a new direction. The process is repeated until a full path is completed. Properties of the wave, for example intensity, wavelength and polarisation, may be altered in the course of the calculation.

Ray tracing can simulate the spatial and temporal characteristics of gravity waves in the atmosphere; many of the important physical effects can be described by the ray equations that track amplitude and trajectory development. The advantages of the technique include: refraction, effects of gravity wave focusing, and local dissipation and response to rapid change in the mean background are taken into account [Lawrence, 2002].

In practice, ray tracing utilises a mathematical model to simulate waves from a source region with spatial and temporal variability and track the propagation and the amplitude evolution to derive the relevant effect of the gravity waves [Lawrence, 2002].

2.6.1 GROGRAT

In 1992, Eckermann developed the method of multi ray tracing as a way to investigate how propagation, filtering and refraction affected gravity waves in the middle atmosphere.

According to the GROGRAT homepage[1], GROGRAT is a four dimensional ray tracing algorithm. GROGRAT stands for "Gravity-wave Regional or Global RAy Tracer". It can trace non-hydrostatic gravity waves through a gridded numerical representation of the Earth's atmosphere. It was developed by Marks and Eckermann in 1995, with updates

[1] http://geospace.nrl.navy.mil/dynamics/html/grograt.html

to the software since then. In short, GROGRAT simulates far-field propagation and amplitude evolution of the gravity waves. On a global scale, it models the propagation and breaking of gravity waves at mesospheric heights [Lawrence, 2002].

The ray tracing model GROGRAT is based on assumes a non-hydrostatic dispersion relation for small-amplitude gravity waves on a slowly varying basic flow
$U = (U(x,x,z), V(x,y,z), 0)$. The atmosphere is assumed to be rotational, stratified and compressible. Sharp gradients in the background wind field are neglected. With the Boussinesq approximation incorporated, and acoustic waves are ignored, the dispersion relation can be written as [Lawrence, 2002]:

$$\omega^{+^2} = (\omega - Uk - Vl)^2 = \frac{N^2(k^2+l^2) + f^2(m^2+\alpha^2)}{k^2+l^2+m^2+\alpha^2} \tag{2.2}$$

where ω is the ground based frequency, ω^{+^2} is the intrinsic wave frequency and (k,l,m) are the wave numbers in respectively the x (east-west), y (north-south) and z (up-down) directions. N is the Brunt-Vaisala frequency, and f is the inertial frequency. $\alpha = a/H_\rho^2$, where H_ρ is the density scale height. Equations 2.2 can be re-written for m as follows [Lawrence, 2002]:

$$m^2 = \frac{(k^2+l^2)(N^2-\omega^{+^2})}{\omega^{+^2} - f^2 - \alpha^2} \tag{2.3}$$

The mixture of positive and negative signs in 2.3 means that, depending upon the wave and atmospheric conditions, the vertical wavenumber can go to 0 or infinity and the wave will cease propagating [Lawrence, 2002].

The GROGRAT model requires the following input data: horizontal wavenumbers (k_0 and l_0), initial height, latitude and longitude, U', and an initial ground based frequency ω_0. The structure of the background atmosphere is supplied via arrays containing U (zonal wind fields), V (meridional wind fields), T (temperature) and P (pressure) data [Lawrence, 2002].

2.7 Geometric Localisation

2.7.1 Epicentre of the Gravity Waves

By fitting the concentric circles to the curvature of the air glow structures, the centre of curvature can be determined, referred to as "the epicentre" from here on. The concept of an epicentre is reasonable if the air glow structures were created by a gravity wave train generated at the point of the epicentre, under the assumption of no background wind [Taylor and Hapgood, 1988].

Based on this principle, the wavefronts will intersect the airglow layer in concentric circles with the source region at the centre. Assuming the structures were created by a linear gravity perturbation at the epicentre, the radii of the observed structures can be calculated and used to find the epicentre [Taylor and Hapgood, 1988].

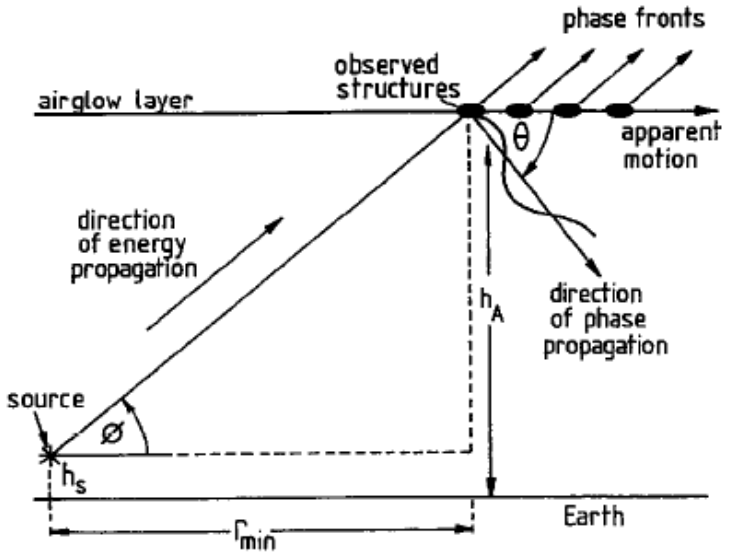

Figure 2.2: Schematic illustration of how a point-like tropospheric gravity wave source generates curved structures in the OH nightglow. For a pure gravity wave $\theta + \phi = 90°$.[Taylor and Hapgood, 1988]

The vertical wavelength, λ_z is assumed to be not larger than the scale height. Under the linear gravity theory of Hines(1960), the group wave fronts of the waves are parallel and upwards inclined at an angle ϕ.

$$\tan(\phi) = [\frac{\tau^2}{\tau_B^2} - 1]^{-1/2} \tag{2.4}$$

Assuming the waves are generated near the Earth's surface, the angle ϕ is the greatest angle of ascent of the wave's energy for a given period. This yields an expression for the minimum range from the source:

$$r_{min} = (h_A - h_S)[\frac{\tau^2}{\tau_B^2} - 1]^{1/2} \tag{2.5}$$

Here, h_A and h_S are the heights of the of the airglow structures and the physical source.

2.7.2 Temporal Origin

The temporal origin can be estimated by calculating the time of flight for the gravity waves from the epicentre to the outer of the airglow structures. Wave energy propagates at the group velocity $v_g = d\omega/dk$, where k is the wavenumber. Taylor and Hapgood [Taylor and Hapgood, 1988] proposed the following relations, under the assumption that the vertical wavelength is not larger than the scale height.

$$k_z^2 = k_x^2[\frac{\omega_B^2}{\omega^2} - 1] \tag{2.6}$$

The horizontal group velocity can be written as:

$$v_{g,x} = \frac{\delta\omega}{\delta k} = \frac{\lambda_x}{\tau}[1 - \frac{\tau_B^2}{\tau^2}] \tag{2.7}$$

2.8 OH Chemistry in the MLT

Sodium can react with oxygen in the MLT to create airglow; as can hydrogen. The hydroxyl layer peaks around 87 km with a FWHM of 5-8 km. The production of the exited hydroxyl state are due to the following set of equations.

$$\mathrm{H + O_3 \rightarrow OH^* + O_2 \ (Rate\ Coefficient\ } k_H) \tag{2.8}$$

Equations 2.9 and 2.10 describe the loss of hydroxyl:

$$\mathrm{H + O_3 \rightarrow OH^* + } h\nu \ \mathrm{(Rate\ A)} \tag{2.9}$$

$$\mathrm{OH^* + M \rightarrow OH\ (Rate\ } K_q) \tag{2.10}$$

In 2.10, M can be O, O_2 or N_2. At steady-state production equals loss:

$$k_h[\mathrm{H}][\mathrm{O_3}] = A[\mathrm{OH^*}] + K_q[\mathrm{M}][\mathrm{OH^*}] \tag{2.11}$$

where [ ] symbolises mean concentration.

$$I_j = [\mathrm{OH^*}]A_j \tag{2.12}$$

Rewriting equation 2.11 to give concentration of exited stated hydroxyl results in the following equation.

$$[\mathrm{OH^*}] = \frac{k_H[\mathrm{H}][\mathrm{O_3}]}{A + K_q[\mathrm{M}]} \tag{2.13}$$

Furthermore, the production and loss of night-time ozone adhere to the following set of chemical equations.

$$\mathrm{O + O_2 + M' \rightarrow O_3 + M'\ (Reaction\ Rate\ } K_O) \tag{2.14}$$

$$H + O_3 \rightarrow OH^* + O_2 \text{ (Rection Rate } k_H) \tag{2.15}$$

Loss and production of ozone must equal for ozone.

$$K_O[O][O_2][M'] = k_H[H][O_3] \tag{2.16}$$

In 2.16, M' is a unspecified third body. Solving 2.16 for $[O_3]$ gives:

$$[O_3] = \frac{K_O[O_2][O][M']}{k_H[H]} \tag{2.17}$$

Substituting the result for $[O_3]$ into 2.13 gives:

$$[OH^*] = \frac{K_O[O][O_2][M']}{A + K_q[M]} \tag{2.18}$$

Thus, as the intensity of a hydroxyl band is given by 2.12, it becomes obvious that the intensity of a hydroxyl band emission is directly proportional to the $[O][O_2]$ product. In other words, the O/O_2 ratio is the direct cause of the OH intensity. A high O/O_2 ratio leads to a high concentration of hydroxyl.[P.Espy, 2012]

2.9 Gravity Waves

Gravity waves are a type of mechanical waves that may arise in several media where gravity works as the restoring force. Generally speaking, gravity waves may occur in any media where the density decreases with height or in the interface between two media with different density, although these are known as surface waves when found, for instance, on the ocean surface, as opposed to the internal gravity waves found in the atmosphere. Sometimes referred to as buoyancy waves, these waves depend on buoyancy in order to exist; the key principle is being that dense matter will rise above matter with lower density and is then restored by gravity.

The waves may be generated in a number of ways. One such way is air flowing over a mountain range. As the waves propagate vertically, their amplitude grows due to energy conservation per unit volume. As the waves reach higher atmospheric altitudes, the neutral density decreases in order to conserve the kinetic energy.

In order to visualise this process, it pays to imagine a corrugated sheet moving though a fluid at velocity c. The movement causes air to oscillate and a wave to propagate away. This explanation, and the associated figures, are taken from Dr. W. Hocking from the University of Western Ontario [W.K.Hocking, 2001].

As can be seen in figure 2.3, at point A the corrugations will be moving forward, forcing the air upwards and forwards, following the purple line in the figure. Thus, air will be compressed, leading to an increase in pressure along this line and making the entire grey area a region of high pressure. At B, it will appear as if the corrugation is moving away. Hence, air in this region will fall, and the broken grey lines will be a region of low pressure.

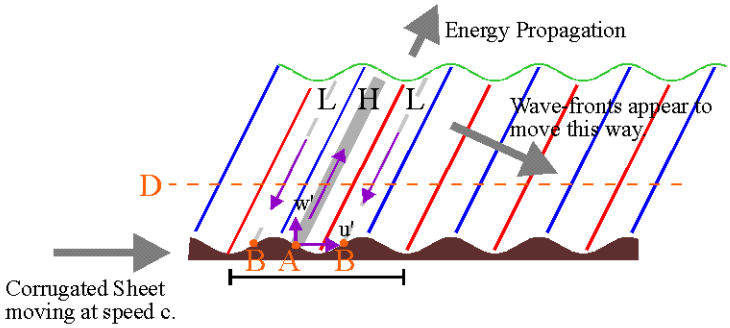

Figure 2.3: Corrugated sheet moving through air

Vertical displacements will follow the corrugations. The upward displacement of the air parcels will be greatest along the blue lines. Adiabatic cooling will cool these air parcels as they rise. On the red lines, the downward displacement will be the greatest. Since the air parcels are sinking here, they will experience adiabatic heating and they will be the hottest parts of the wave.

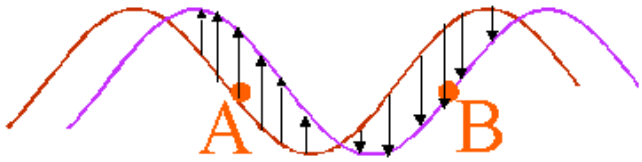

Figure 2.4: Movement of points A and B

The wavefronts move with the corrugations. To an observer they will appear to follow the grey arrow sloping down and to the right, moving with the phase velocity of the wave. The energy propagation will move up to the right, as was the air at point A. This is the reason for the waves being able to carry energy up in the atmosphere.

Then there is also the question of the stability of the atmosphere to consider. At the top of the oscillation, the air is cooler than its surroundings; the mark of a stable atmosphere. At the bottom of the oscillation, the air parcel will be warmer than its surroundings and it will rise again. Consequently, gravity wave propagation require a stable atmosphere.

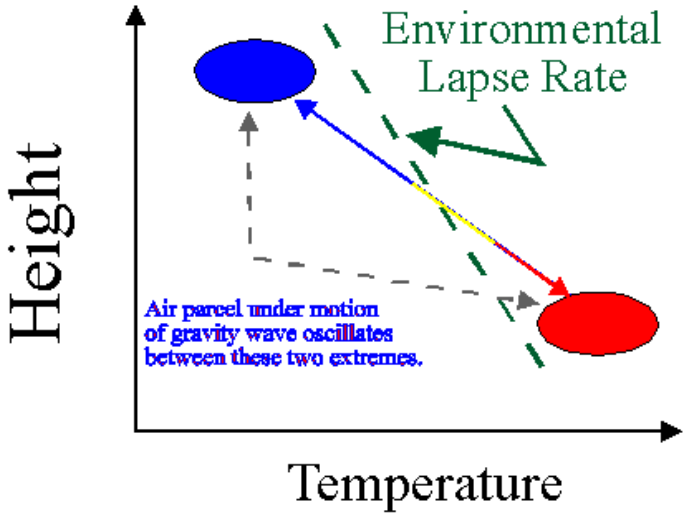

Figure 2.5: Adiabatic lapse rate

If a gravity wave is generated in a stable part of the atmosphere and it propagates upward, it may come to encounter an unstable region of the atmosphere. The waves will not be able to pass this region and will bounce back, depositing much of the energy. Likewise, should the waves encounter a region in which the wind speeds of the background exceed the phase velocity of the gravity waves, further upward propagation will be impossible. The result is popularly referred to as a "sonic boom"; the amplitude grows very large due to the wave moving along with the air. Eventually, the wave breaks down and destroys itself, dumping momentum and energy into the surrounding atmosphere.

For better understanding these motions, the Brunt-Vaisala frequency is introduced.

$$\tau_B = \frac{2\pi}{\sqrt{\frac{g}{T}(\Gamma_a - \Gamma_e)}} \tag{2.19}$$

T is mean temperature, Γ_a is the adiabatic lapse rate and Γ_e is the environmental lapse rate. This period corresponds to the period if an air parcel is displaced and allowed to oscillate freely. The Brunt-Vaisala frequency can be used to relate the horizontal and vertical wavelength of the gravity waves. The intrinsic horizontal phase speed is $c_{int} = \frac{\lambda}{T}$, where λ is the wavelength and T is the period.

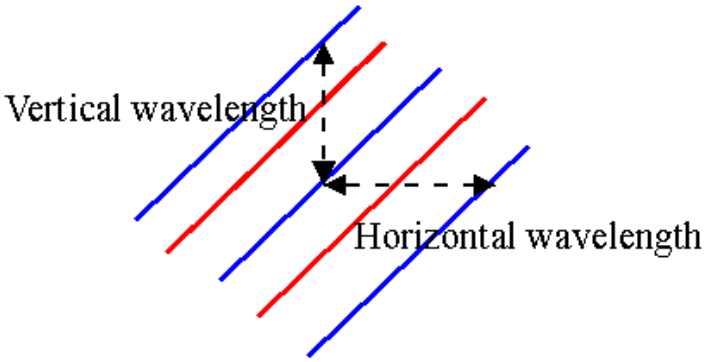

Figure 2.6: Horizontal and vertical wavelength

The horizontal wavelength is by definition the horizontal distance between identical wave-fronts. Similarly, the vertical wavelength is the vertical distance between identical wave-fronts. Generally speaking, horizontal wavelengths are much longer than the vertical ones; vertical wavelengths being on the order of a few hundred metres to a few tens of kilometres while the horizontal wavelengths can be as long as hundreds and thousands of kilometres. As promised above, the following equation relates the horizontal and vertical wavelengths:

$$\frac{\lambda_H}{\lambda_V} = T \tag{2.20}$$

Here, λ_H is the horizontal wavelength and λ_V is the vertical wavelength. It is worth noting that equation 2.20 is invalid for very short or very long periods.

For observing gravity waves in the MLT, this project focuses on taking pictures of the airglow with an all-sky CCD camera with a suitable filter in place. The resulting image is a picture of the airglow intensity across the sky. Variations are due to vertical displacement of air parcels by the gravity waves. The air here is subject to adiabatic processes; air that rises is subject to adiabatic expansion and is cooled, while the sinking air is subjected to adiabatic compression and is heated. The species involved in the airglow producing reactions - such as O, H and O_2 - have mixing ratios that vary greatly with height. A vertical displacement will produce a significant change in the concentration. It is worth noting that airglow observations are best suited to observation of waves with vertical wavelength $\lambda_z > 12$ km. This is waves with wavelengths longer than the airglow layer. The horizontal wavelength should be confined within the field of view, i.e $\lambda_x < 300$ km.[Plane, 2003]

2.10 Potential Sources of Gravity Waves

The primary focus of this thesis is gravity waves being generated by sources in the lower atmosphere that propagates upwards to mesospheric heights where they can be observed in the OH nightglow. Not all gravity waves are generated in the lower atmosphere, and a fair amount of the gravity waves that can be seen in the OH airglow images might be the remnants of other waves that have broken down.

Many phenomena may cause gravity waves. Meteorological disturbances is one cause; thunderstorms is a well-documented cause of gravity waves at low and middle latitudes. At high latitudes, auroral activity may contribute. Frontal systems is another. In Norway orographic activity is particularly relevant, since Norway is the first mass of land eastward winds encounter as they blow in over Scandinavia. Norwegian topography could be described as relatively high mountains rising from the ocean in the west and a gradual slope to the east. Sporadic sources also exists, but they are not very relevant to the results of this thesis.

2.11 Convective Activity

Gravity wave theory predicts that isolated, sufficiently convective thunderstorms can launch waves and create a unique intensity pattern of concentric circles on a radiating surface of constant altitude above such a storm [Dewan et al., 1998].

2.11.1 Gravity Wave Generation by Auroral Activity

There are two mechanism that would allow for gravity waves to be generated by auroral activity: the Laplacee force $(\vec{J} \times \vec{B})$ set up by the electric currents of the auroral electrojet and exerted on the neutral air in the E-region, and heating of the neutral air, due to the Joule effect of the electrojet or particle precipitation [TESTUD, 1970].

2.11.2 Gravity Waves by Topographic Launching

Mountain waves are generated by air-flow over topography [Schoeberl, 1985]. There are both stationary mountain waves with zero horizontal phase speed [Schoeberl, 1985], and freely propagating mountain waves with phase velocities different from zero. Mountain wave generation in northern Scandinavia form mainly under foehn-like weather conditions.[Dörnbrack et al., 2002].

A disturbance is created when stably stratified air is forced to flow over a topographic barrier, and the associated energy is usually carried away in the form of gravity waves. This type of gravity waves are called mountain waves.[Durran, 1990]

Section 4.8 provides a more thorough explanation on how waves of this type are generated and propagate to mesospheric height.

2.11.3 Non-Orographic Gravity Wave Sources

Examples of non-orographic sources include: mid-latitude frontal systems, upper-level jets, dry-boundary layer convection and deep tropical convection [Lane et al., 2001]. Zones of the deep tropical convection are the dominant sources of convectively generated gravity waves and possibly the most important sources of high frequency gravity waves on the Earth [Vadas and Fritts, 2004].

2.11.4 Sporadic Sources

Sporadic sources include volcanic eruptions, earthquakes, solar eclipses, auroral activity, meteorites, nuclear and chemical explosions, supersonic jets, spacecraft launches and other sporadic events. Previous studies have succeeded in tracing gravity waves back to sporadic sources. The volcano of Okmok erupted in 2008 with evidence of gravity wave activity caused by this event [Angelis et al., 2011].

2.11.5 Mesospheric Bores

Rather than being the cause of a gravity wave, mesospheric bores are often caused by gravity waves depositing momentum into an atmospheric "funnel". However, it is highly possible that a portion of the waves that are observed in the airglow images may in fact be secondary waves, or in some cases mesospheric bores. Therefore this section provides a brief explanation of the phenomenon.

Mesospheric bores, is a comparable to tidal bores in rivers and the ocean. Such tidal bores is when a large wave crest or a series of wave crests travel upstream in a river or an estuary as the result of a tidal surge. [Smith et al., 2003]

Bores can also occur in the mesosphere; Dewan and Picard [Dewan and Picard, 2001] suggested that the bores may be due to interaction between gravity waves/critical layer and the mean background wind, and that the resulting inversion layer and the bore share the same origin.

However, there are major differences between the tidal bores and the mesospheric bores; tidal bores are *surface* bores whereas the mesospheric bores are what is known as *internal* bores. The four main differences between the two are: (1) internal bores can be stronger than surface bores before breaking occurs, (2) the acceleration of gravity must be modified to the buoyant acceleration for internal bores, (3) the possibility of mixing of the lower and upper fluid, and (4) under certain circumstances, waves can carry energy vertically from an internal bore thus providing and additional source of dissipation. [Dewan and Picard, 1998]

The question regarding internal bores is what fulfils the role as a duct or a funnel. It is not as straight-forward as for the tidal bores. It is clear that it must be a region of higher stability bounded on both sides by regions of a lower level of stability; specifically

a temperature difference over an inversion layer. Interactions between a gravity wave and a critical layer has with momentum accelerating the mean flow to instability has could possibly be a mechanism responsible for producing such a region, with turbulence and subsequent heating. [Dewan and Picard, 2001]

2.11.6 Evanescent Waves

Many of the waves being run in the GROGRAT model are *evanescent*. Evanescent means "tending to vanish", which is appropriate considering that the intensity of an evanescent wave decays exponentially. Evanescent waves are created when a wave is internally reflected off an interface at an angle greater than the critical angle so that total internal reflection occurs. An evanescent wave will therefore not propagate wave energy upward and will instead be "ducted", sometimes over long distances, by the waveguide.

In short, evanescent waves are waves that are not propagating. When GROGRAT returns the output of an evanescent wave, it means that the wave is not a wave that has its source in the lower regions of the atmosphere and has propagated upwards from there, but rather the remnants of a gravity wave having broken down and deposited its momentum in the mesosphere. To sum up, they are impossible to trace back to the source regions via GROGRAT.

CHAPTER 3
METHOD

3.1 Data Analysis

This section gives a brief explanation on how the GROGRAT input data has been calculated from the OH nightglow images, and how the geometric localisation was carried out.

3.1.1 Directions in the Airglow Images

It is common practice to align the images in such as way that north points upwards and east is to the right. However, aligning the images in such a way requires extensive cropping. Since the field of view is already fairly limited, and the mapping code already removes a substantial of the image, it was decided that this alignment was not necessary.

The position of Stellar Polaris was used to find north in the airglow images. It is generally a difficult task to use the stars in the night-time sky to find the directions in the nightglow images because of the filter transmittance. The filters only transmit light of a certain frequency range. Consequently, determining the magnitude of the stars is made very difficult, as stars whose spectral lines has frequencies that correspond with the light that is transmitted by the filters will look much bigger than they might appear to the naked eye in the night-time sky. Similarly, if the star's spectrum is such that it emits little light with frequency within the bandwidth of the filter, the star might appear fainter than it is. Identifying single stars or even constellation in the airglow images is therefore a near impossible task with a regular star map which only gives magnitudes for the full spectrum of the star.

However, Stellar Polaris has that unique property that it barely moves relative to an observer on the surface of the Earth and points almost exactly to the north at all times. The

the airglow images were made into videos, and the star that remained stationary throughout the night is the Stellar Polaris. Its coordinates in the images were kept and used as the coordinates indicating north.

The coordinates of the zenith are know from the mapping code. South was taken to lie opposite if north through zenith, and the east-west axis is perpendicular to the north-south axis. Looking again at the direction of rotation in the airglow images, east and west become apparent, since the stars rotate from east to west.

3.1.2 Ray Tracing Data

GROGRAT requires the following input: wavenumbers k and l, U' and ω_{obs}, as well as longitude and latitude and atmospheric height for the waves. The information necessary to find the input is collected from the OH airglow images, where the relevant physical variables needed to calculate the GROGRAT input data are: horizontal wavelength, amplitude, intrinsic phase speed, background intensity value. In addition, the method relies on a cancellation factor, based on intrinsic phase speed and background winds.

Finding wavelength, amplitude and phase speed from the airglow images is done in Matlab, by a form of sine fitting on the intensity variations in OH airglow images, which is sinusoidal in nature, as are the gravity waves. The method requires a series of consecutive images with a clear sine form and little disturbance and relatively straight wavefronts. Most of the clear nights this winter do show distinct gravity wave structure in the airglow for long periods of time. However, most of these waves are very difficult to analyse; often there is too much disturbance in the images (often two gravity waves coming in from different directions and creating a "grid" pattern in the airglow, or a wave breaking similar to a ocean wave breaking on the beach). Sometimes the amplitudes are faint compared to the background so that the signal to noise ratio is too small to get a good result with the fitting. Many waves observed in the airglow are only stable stable for a relatively short period of time. There are 180 seconds between each OH image (from the beginning of one to the beginning of the next). For many waves, there is only clear sinusoidal structure for 2-3 images.

The Matlab code[1] that does the sine fitting works in two steps; (1) it first maps the airglow images to geographic coordinates, so that a certain number of pixels corresponds to a certain length in meters, and (2) based on input pixel coordinates for a start and an end point, the code will find the shortest wavelength, and return wavelength, amplitude, phase and the direction of propagation. The process of finding the shortest wavelength is to do a "sweep" around the start vector. The reason for choosing the shortest wavelength is that within reason it can be assumed that this vector is perpendicular to the wavefronts. The wave is also assumed to propagate in this direction.

[1] The code was written by Morten Hatlen

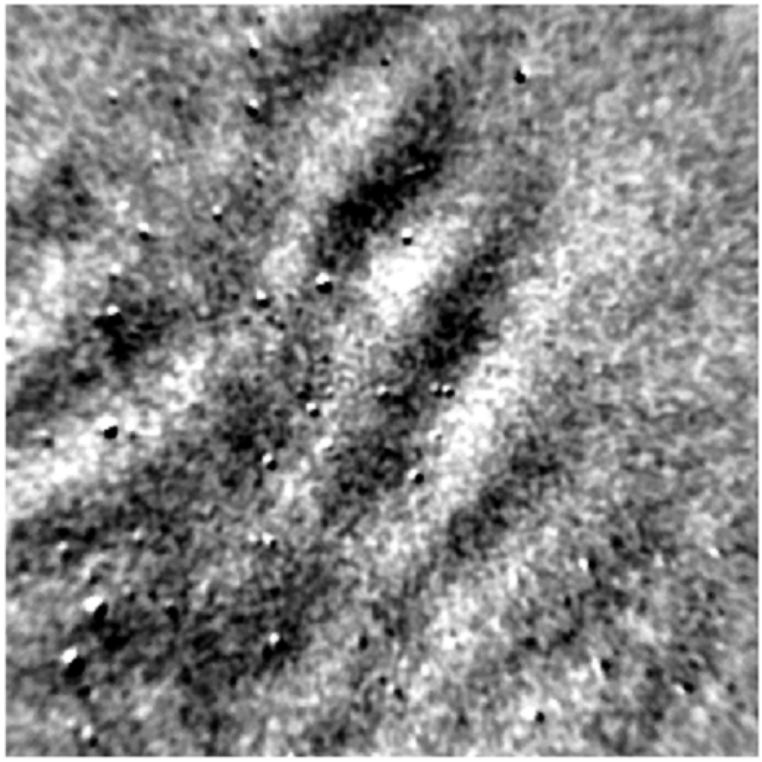

Figure 3.1: A gravity wave in the OH airglow images on 7th feb.taken around 23:40 UTC.

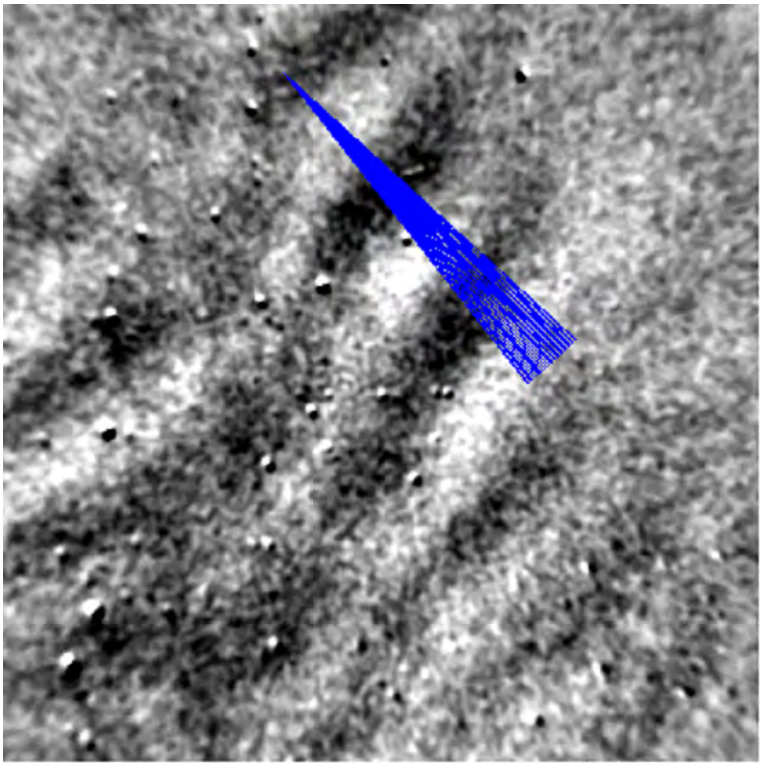

Figure 3.2: A gravity wave in the OH airglow images on 7th feb.taken around 23:40 UTC with the "sweeping" mechanism

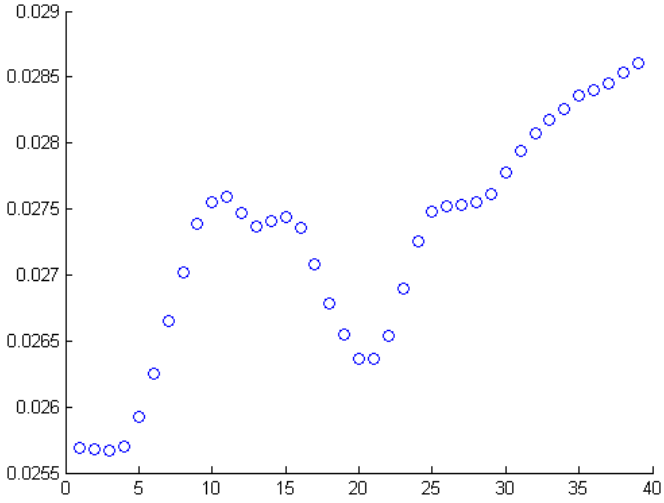

Figure 3.3: A scatter plot of the different wavelengths (in pixel values)

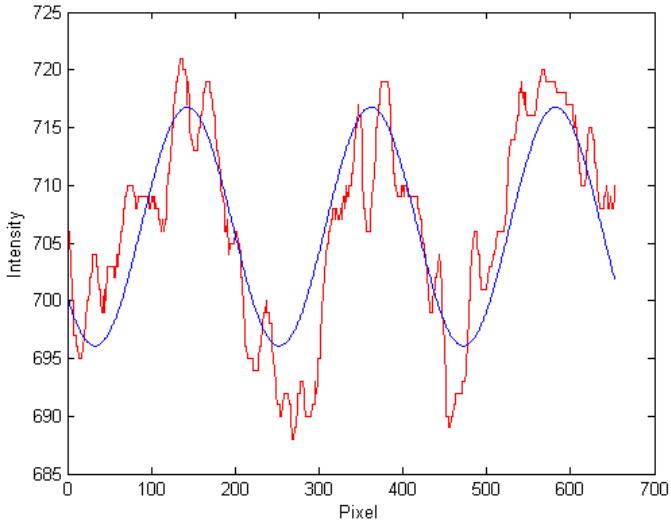

Figure 3.4: How the fit works relative to the intensity data.

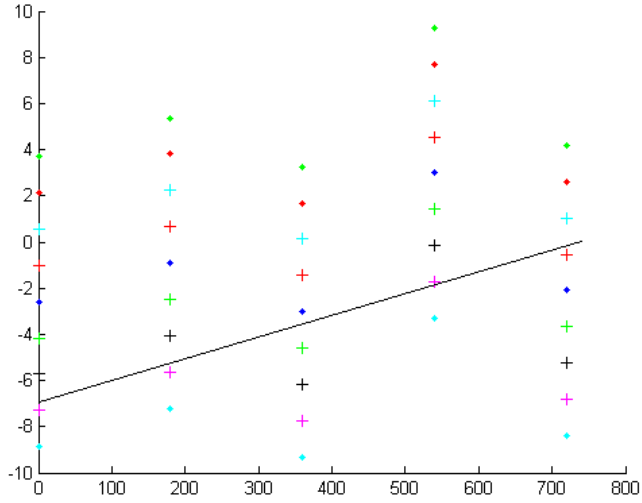

Figure 3.5: Plot of the phases(blue dots) plus/minus multiples of 90°

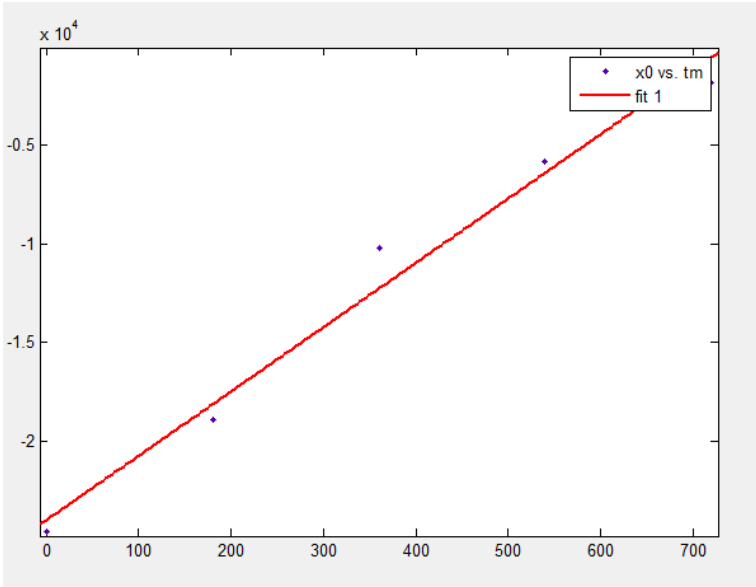

Figure 3.6: Plot of selected phases and the fitting

The signal to noise ratio in the OH airglow images are improved by subtracting two subsequent images. This subtraction is accounted for in the amplitude calculations as one would by subtracting two sine functions. The other reason for subtracting the OH airglow images is that it removes the filter function; in the raw OH airglow images the intensity is greatest in the centre of the image and falls rapidly at the edges. This creates problems with finding an accurate amplitude value. The average value of wavelength and amplitude are used in the final calculations. The phase speed is calculating by linearly fitting the phase values. The sine fitting returns phase values in different quadrants; this is remedied by adding/subtracting multiples of $\pi/2$ to the phase array and plotting all the values in the same plot. The set of values for the phase that best corresponds to the approximated value that can be observed as the wave propagates in the airglow images is chosen.

3.1.3 Geometric Localisation

Only a few waves exhibit a distinct curved wavefront. Most of the waves have wavefronts that at least *appear* straight; there is a distinct possibility that many of the straight wavefronts that can be seen in the airglow images are in fact curved, but that the field of view (of 45°) is too small for it to be possible to discern this curvature in the airglow images. Consequently, the waves whose wavefronts do display a distinct curvature, have to a relatively small radius of curvature. It therefore follows that these waves have an epicentre that is relatively close. There are no such restrictions on the ray tracing method.

A series of points that represent the curvature of the wavefront is fitted and plotted on top of the airglow images similar to figure 3.7. Figure 3.7 shows the airglow structures mapped geographically and their geographic epicentre. Figure 2.2 shows how gravity waves generated in the lower atmosphere propagate upwards to mesospheric heights. r_{min} is the horizontal distance from the airglow structures to the epicentre. This distance is found in the fitting process.

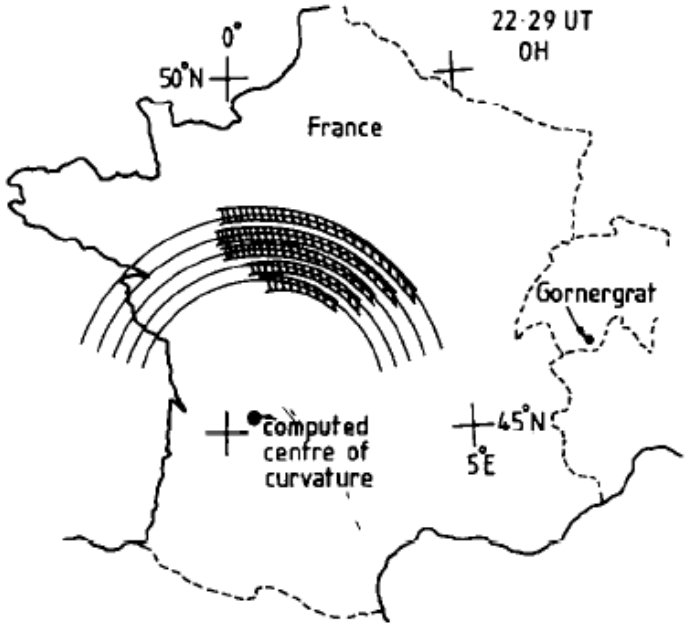

Figure 3.7: Ground map of the OH nightglow structures Taylor and Hapgood [1988].

3.2 GROGRAT

GROGRAT has several different kinds of output after it has processed the input. *Integration failiure* happens when the rays are numerically unstable and should have been terminated earlier. Sometimes, the waves break the WKB criteria in the vertical direction. This usually happens at critical layers, but also when the WKB approximations are violated, which often happens when the properties of the medium vary slowly on a scale comparable to wavelength. *Evanescent* waves are waves that do not propagate, meaning that they could not have originated in the lower atmosphere and propagated upwards, but is more likely a remnant of a wave that has broken down at mesospheric heights. Note that GROGRAT is only running the downward direction, for waves propagating upward. This means that waves generated higher up in the atmosphere and is downwards propagating, such as waves created by auroral activity, cannot be traced by this scheme [Lawrence, 2002].

In addition to the input wave parameters for GROGRAT, GROGRAT also requires a set of input arrays that contain all the information about the background atmosphere at the time of the wave. GROGRAT requires 4 such arrays: temperature, zonal and meridional wind field, and pressure or height. These fields have been generated using the empirical models MSISE-90 [Hedin, 1991] for temperature and pressure, and HWM-93 [Hedin et al., 1996] for horizontal winds. For this thesis, pressure fields have been used for the GROGRAT ray-tracing. The arrays stretch from sea level up to a 100 km in the atmosphere; this is sufficient since the OH airglow layer is located at about 87 km. The arrays have 51 vertical steps with a 2 km spacing between them.

Calculating the four GROGRAT parameters are fairly straightforward. k_0 and l_0 are the horizontal wavenumbers.

$$k_0 = \frac{2\pi}{\lambda \sin(\theta)} \tag{3.1}$$

$$l_0 = \frac{2\pi}{\lambda \cos(\theta)} \tag{3.2}$$

In equations 3.1 and 3.2, θ is the angle between north and the direction of propagation in the, with positive angles towards east. Then there is the angular frequency of the wave:

$$\omega_{obs} = \frac{2\pi c}{\lambda} \tag{3.3}$$

In equation 3.3, c is the phase speed. Finally, then there is U':

$$U' = \frac{g}{\tau_{BV}} \cdot CF \cdot \frac{A}{A_0} \tag{3.4}$$

Here, g is the gravitational acceleration, taken to be 9.8m/s^2, τ_{BV} is the Brunt-Vaisala frequency at 0.02 rad/s, CF is a cancellation factor which the following section will focus on. A is the amplitude of the wave, and A_0 is the background intensity [P.Espy, 2013].

3.2.1 Cancellation Factor

The Horizontal wavelength is used to estimate the vertical wavelength, see figure 3.9, and this is used to estimate the cancellation factor, see figure 3.8. As mentioned, the waves passing through the $\sim$8 km thick airglow layer have to have vertical wavelengths greater than about 12 to 16 km to be observed. Thus, it can be seen in Figure 15 that the cancellation factor for these waves is nearly constant.

Equations **??** and **??** are used to calculate the cancellation factor in equation 3.4. Figures 3.8 and 3.9 gives a graphic representation on how the cancellation factor varies as a function of the observed parameters c_0 and λ_x.

Figures 3.8 and 3.9 illustrate how the cancellation factor is found.

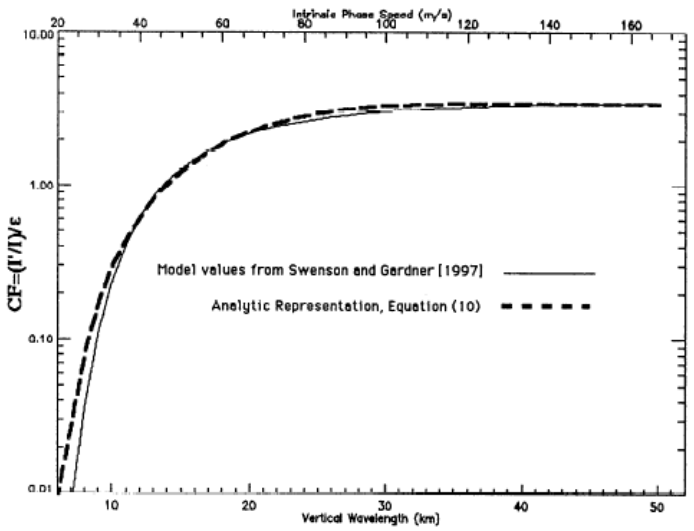

Figure 3.8: A plot of cancellation factor versus vertical wavelength Swenson and Liu [1998]

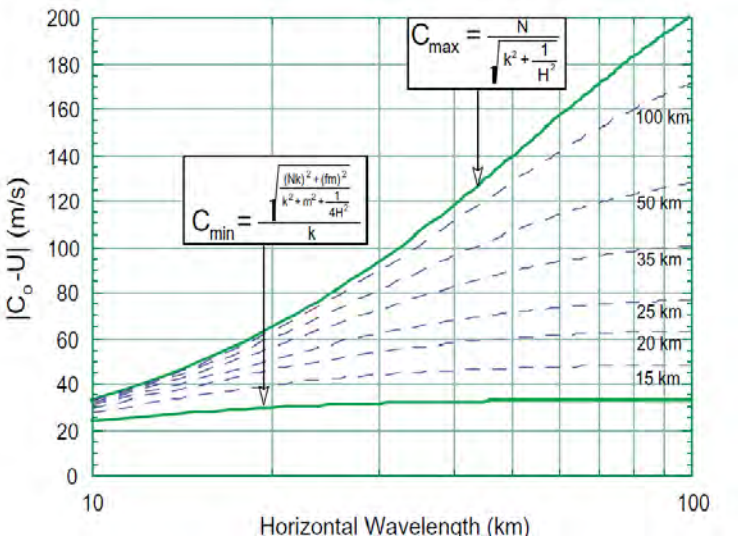

Figure 3.9: A plot showing vertical wavelength as a function of horizontal wavelength and intrinsic phase speed Swenson et al. [2000]

3.2.2 Background Intensity

Several methods were tried and tested to find a measure of the background intensity on the nights in question. In the end a method which added several (between 70 and 100, depending on how many images that was undisturbed by clouds and moonlight. Both will increase the background intensity of the images.) images from a clear part of the night together which then averaged the image intensity was settled on, and the "dark" intensity was subtracted. Then for a small area somewhere close to the zenith of the images, the average intensity was calculated. The "dark" intensity is the intensity the camera adds to the images; if the shutters of the camera were closed, the images would still show a certain intensity. For the camera system, this intensity is $\sim$3000.

3.2.3 Amplitude Calculations

$$A' = \frac{A}{2\sin(\frac{\pi \cdot c \cdot \Delta T}{\lambda})} \tag{3.5}$$

In equation 3.5, ΔT is the time between the beginning of two OH airglow images. c is the observed phase speed, λ is the observed wavelength and A is the observed amplitude in the subtracted images.

3.2.4 Horizontal Wind Model 1993 (HWM93)

The background wind arrays are generated from the Horizontal Wind Model from 1993, hereafter referred to as the HWM93 [Hedin et al., 1996]. The HWM93 is an global empiri-

cal model of the horizontal winds in the upper and middle atmosphere. The model is based on data from satellite measurements, radar and ground-based optical remote sensing. A limited set of vector spherical harmonics is used to describe the zonal and meridional wind components. The model includes solar cycle variations. As are variations with magnetic activity. The model is particularly good for low and mid latitudes. The polar vortices are also included in the model, but not in full detail, which lowers its accuracy at polar latitudes.

The model represents time-varying means and tidal components in the lower, middle and upper atmosphere. Similar to the HWM93, the Mass Spectrometer-Incoherent Scatter Extended empirical model from 2000 (MSISE-00) is used to generate the temperature and pressure fields. Fourier and vector spherical harmonic interpolation and extrapolation is used. The required inputs in the model are: day of year, local time, latitude, longitude and altitude, solar flux and geomagnetic activity.

From experience, GROGRAT is very sensitive to changes in the background wind field. At Trondheim latitudes, the mesospheric tides are very strong , and changes in the background wind field can occur quite rapidly. Figure 3.10 shows how the winds at different altitudes in the mesosphere changes with the tidal waves in the region. As mentioned, background winds are responsible for filtering effects. Consequently, within the time span of the propagation of a wave across the imager field of view, the background winds may have changed significantly, and running the HWM93 for the beginning and the end times may yield very different results should this coincide with a tidal wave coming in.

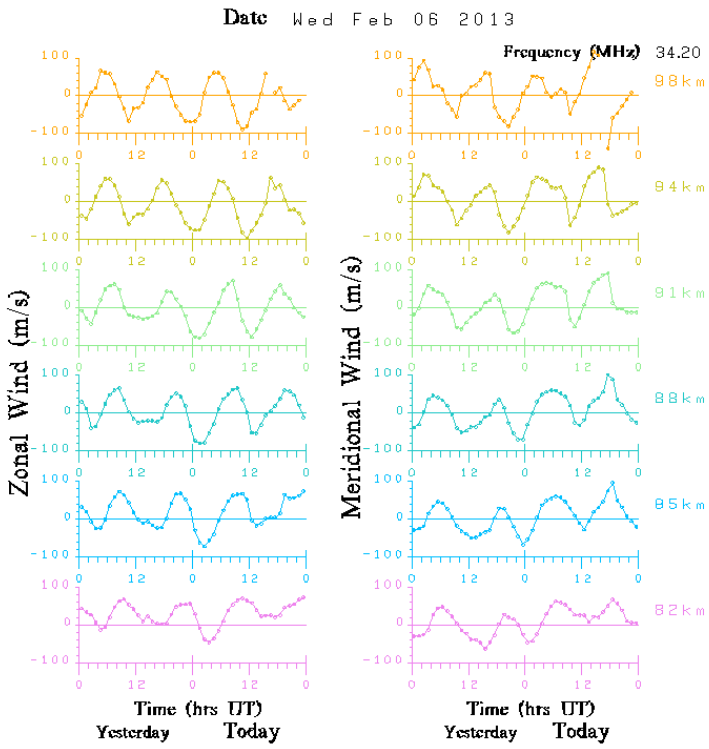

Figure 3.10: Background horizontal winds at mesospheric heights on February 5. and 6. Positive directions indicate north and east, as per convention. Observe how the winds may change by as much as 150 m/s over a period of 6 hours. (February 6. at 85 km)

Figure 3.10 is taken from the homepage of the NTNU atmospheric physics group[2].

In fact, the most common way of ray-tracing with GROGRAT is to trace rays upwards; several waves with different wavelengths and phase speeds are run simultaneously to test which combinations are filtered at critical layers and which combinations will reach mesospheric heights. This paper attempts a different approach.

[2]http://home.phys.ntnu.no/brukdef/prosjekter/atmosfys/web-pages/main.php

CHAPTER 4
RESULTS

4.1 GROGRAT Results

The first part of this thesis is focused on the ray-tracing as performed by GROGRAT. GROGRAT performs the ray-tracing using a few input parameters on the gravity waves and returns the geographic coordinates of the source if the parameters are such that GROGRAT is capable of tracing the waves. If for some reason GROGRAT is incapable of conducting the ray-tracing, an output of what went wrong in the process; it can be an integration failure or reflection off a critical layer in the atmosphere. Sometimes the waves are *evanescent*, meaning that the waves do not propagate.

Figure 4.1 shows the geographic location of the gravity waves sources as calculated by GROGRAT. Table 4.1 displays the GROGRAT output for the waves. longitude and latitude are given in decimal degrees. North and East are defined to be positive coordinates. An *evanescent* wave means that the wave does not propagate. These waves are impossible to trace with GROGRAT. A *dissipating* wave is a wave whose amplitude gets decreases until the wave is practically attenuated. These wave are being traced back to its geographic origin with GROGRAT. Figures 4.2 shows the different phase speeds, wavelength, U' values and periods.

Table 4.1: Coordinates and altitude of the gravity wave sources as calculated by GROGRAT

wave	Latitude	Longitude	Atmospheric Height (km)	Traceable
1	63.46	9.807	15.74	Dissipating Wave
2	61.04	11.62	15.38	Dissipating Wave
3	62.89	9.500	4.778	Dissipating Wave
4	63.02	9.451	18.25	Dissipating Wave
5	58.01	12.48	3.760	Dissipating Wave
6	62.25	11.84	4.302	Dissipating Wave
7	63.36	10.01	19.25	Dissipating Wave
8	61.72	11.33	12.98	Dissipating Wave
9	63.01	10.30	19.61	Dissipating Wave
10	-	-	-	Evanescent Wave
11	-	-	-	Evanescent Wave

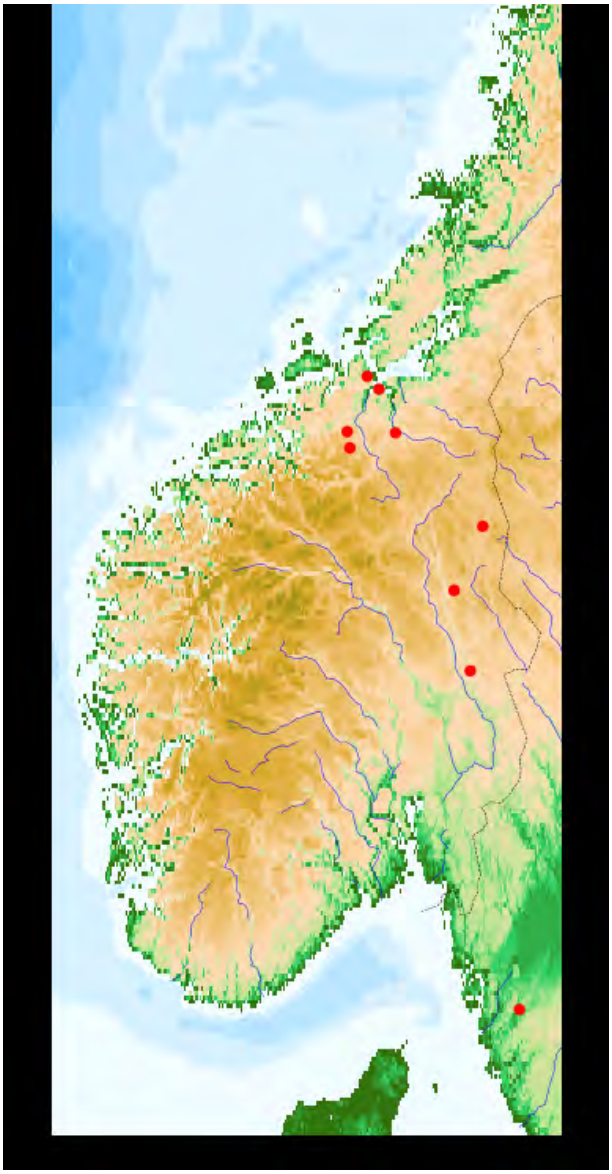

Figure 4.1: Geographic location of the non-evanescent waves from GROGRAT

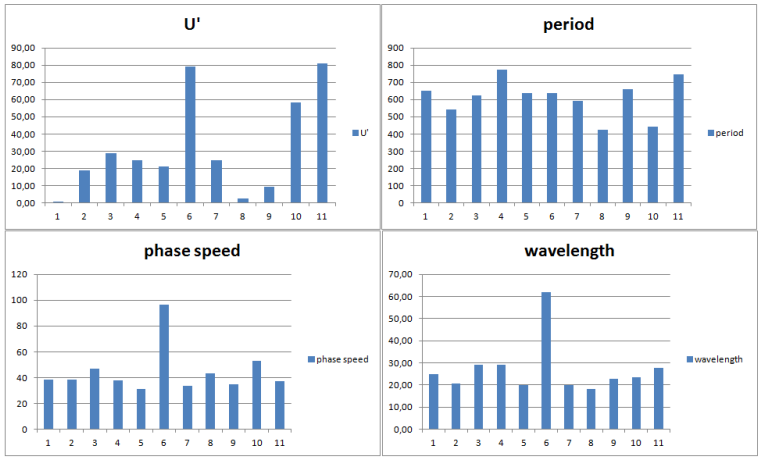

Figure 4.2: Histogram representation of the different wavelengths, periods, phasespeeds and U' values for GROGRAT analysis. Wavelength has km as vertical axis, phase speed has m/s, period has seconds and U' has m/s.

4.1.1 wave 1

This wave is from December 6, around 18:00 UTC and 19.00. According to the GROGRAT ray-tracer, this wave dissipates at an atmospheric height of 15.74 km, somewhere in the lower stratosphere or tropopause. The geographic coordinates are (63.46°, 9.807°). This puts the wave source west of Trondheim, just a little further out the fjord.

4.1.2 wave 2

This wave is from January 16, around 01:00 UTC. According to the GROGRAT ray-tracer, this wave dissipates at an atmospheric height of 15.38 km, of about the same atmospheric heights as the tropopause/beginning of the stratosphere, and at the coordinates (61.04°, 11.62°).

4.1.3 wave 3

This wave is from January 16, around 19:15 UTC. According to the GROGRAT ray-tracer, this wave dissipates at an atmospheric height of 4.778 km and at the coordinates (62.89°, 9.500°). The source of this wave lies in the middle of the mountain range Trollheimen. This wave traces further down, into the troposphere.

4.1.4 wave 4

This wave is from February 9, around 22:00 UTC. According to the GROGRAT ray-tracer, this wave dissipates at an atmospheric height of 18.25 km and at the coordinates (63.02°, 9.451°). The geographic location of the this gravity wave source is close to the source of wave 4.

4.1.5 wave 5

This wave is from February 7, around 23:30 UTC. According to the GROGRAT ray-tracer, this wave dissipates at an atmospheric height of 3.760 km and at the coordinates (58.01° 12.47°).

4.1.6 wave 6

This wave is from March 30, around 19:30 UTC. According to the GROGRAT ray-tracer, this wave dissipates at an atmospheric height of 4.302 km and at the coordinates (62.25° 11.84°).

4.1.7 wave 7

This wave is from February 9, around 23:00 UTC. According to the GROGRAT ray-tracer, this wave dissipates at an atmospheric height of 19.25 km, coordinates (63.36° 10.01°).

4.1.8 wave 8

This wave is from February 8, around 05:00 UTC. According to the GROGRAT ray-tracer, this wave dissipates at an atmospheric height of 12.98 km, coordinates (61.72° 11.33°).

4.1.9 wave 9

This wave is from November 18 2012, around 01:00 UTC. According to the GROGRAT ray-tracer, this wave dissipates at an atmospheric height of 19.61 km, coordinates (63.01°, 10.30°).

4.1.10 wave 10

This wave is from December 3 2012, around 18:00 UTC. This wave is evanescent according to GROGRAT.

4.1.11 wave 11

This wave is from January 17 2013, around 02:00 UTC. This wave is evanescent according to GROGRAT.

4.2 Geometric Localisation

The second part of this thesis focuses on on waves with curved wavefronts. It assumes that waves with curved wavefronts have sources in the lower atmosphere (troposphere) that generates a wavetrain with the source at the epicentre. Due to the field of view of the camera, as well as cropping done by the mapping code, the area of observations is quite limited. It makes it hard to observe the curvature of waves whose radii is large compared to the area of observation.

4.2.1 03.12.2012

On December 3 2012 from $\sim$ 18:00 UTC to 19:00 UTC, it was possible to discern a curvature of the wavefronts. Four consecutive images that best showed this curvature without disturbance were selected for analysis. The results of the fitting are summarised in table 4.2

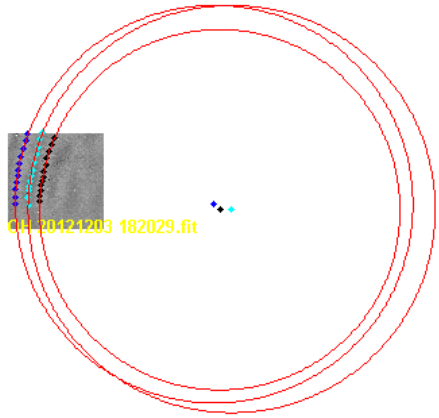

Figure 4.3: Airglow image with fitted circles and their epicentre

This gives the respective distances from the zenith of the of image of 163 km, 182 km, 170 km and an angle between north and the centre of the circle of 25°, 24° and 23°.

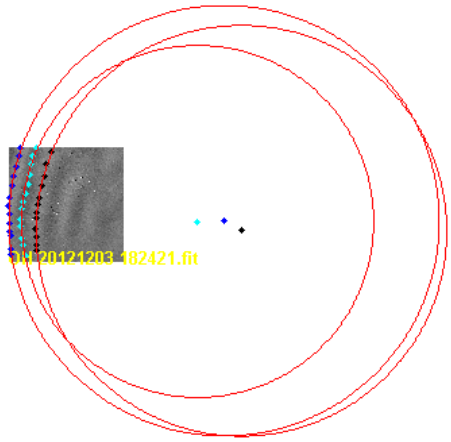

Figure 4.4: Airglow image with fitted circles and their epicentre

This gives the respective distances from the zenith of the of image of 134 km, 111 km, 150 km and an angle between north and the centre of the circle of 27°, 25° and 25°.

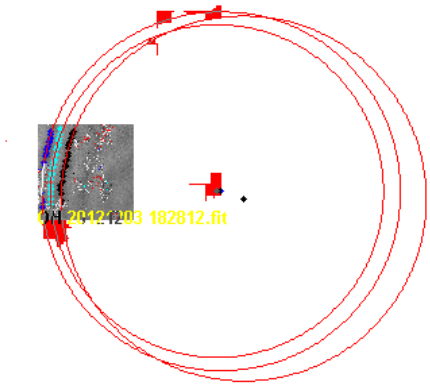

Figure 4.5: Airglow image with fitted circles and their epicentre

This gives the respective distances from the zenith of the of image of 139 km, 135 km, 164 km and an angle between north and the centre of the circle of 25°, 25° and 24°.

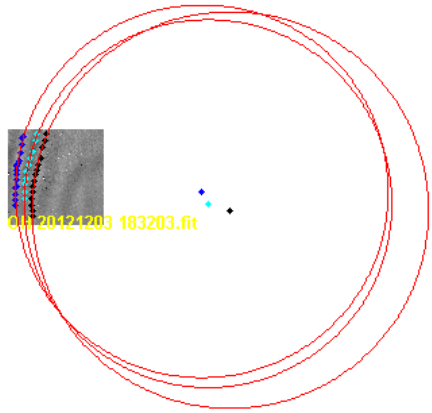

Figure 4.6: Airglow image with fitted circles and their epicentre

This gives the respective distances from the zenith of the of image of 150 km, 158 km, 182 km and an angle between north and the line from zenith to the centre of the circle of 28°, 23° and 22°. This is to the north west of Trondheim.

Table 4.2: Geographic location of the observed gravity waves

Distance (km)	Angle (deg)
163	25
182	24
170	23
134	27
111	25
150	25
139	25
135	25
164	24
150	28
158	23
182	22

4.2.2 16.01.2013

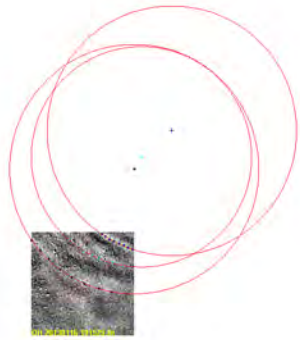

Figure 4.7: Airglow image with fitted circles and their epicentre at 16.jan 2013

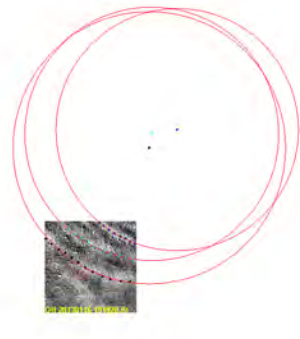

Figure 4.8: Airglow image with fitted circles and their epicentre at 16.jan 2013

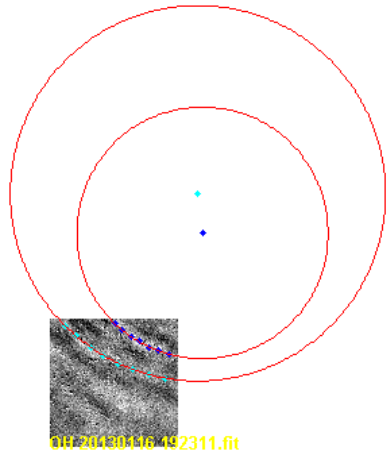

Figure 4.9: Airglow image with fitted circles and their epicentre at 16.jan 2013

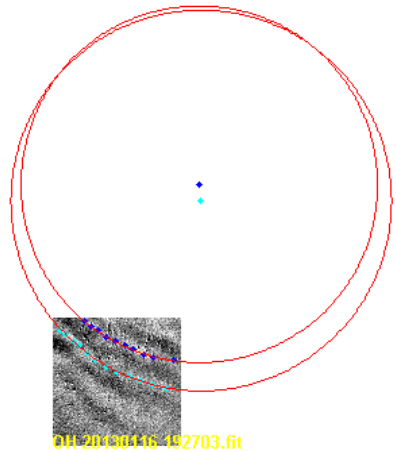

Figure 4.10: Airglow image with fitted circles and their epicentre at 16.jan 2013

Figure 4.11: Airglow image with fitted circles and their epicentre at 16.jan 2013

Table 4.3: Geographic location of the observed gravity waves

Distance (km)	Angle (deg)	Direction of angle
170	4	south of west
134	10	south of west
120	11	south of west
175	2	south of west
158	10	south of west
143	8	south of west
134	4	south of west
160	10	south of west
165	12	south of west
154	9	south of west
192	9	south of west
201	8	south of west

4.2.3 17.01.2013

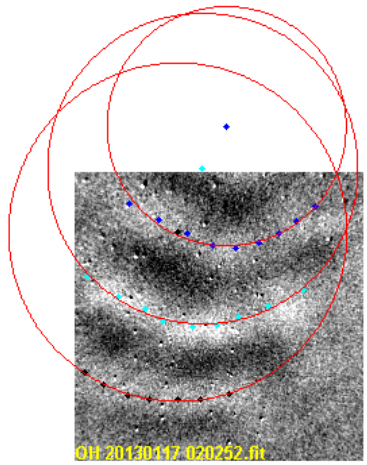

Figure 4.12: Airglow image with fitted circles and their epicentre at 16.jan 2013

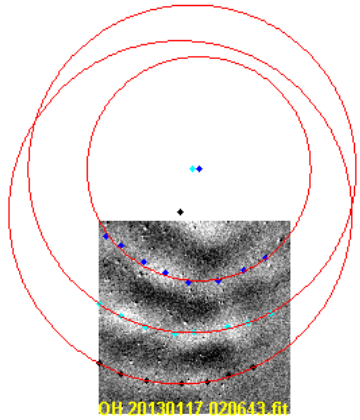

Figure 4.13: Airglow image with fitted circles and their epicentre at 16.jan 2013

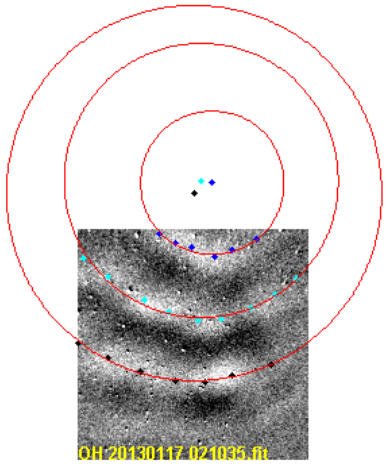

Figure 4.14: Airglow image with fitted circles and their epicentre at 16.jan 2013

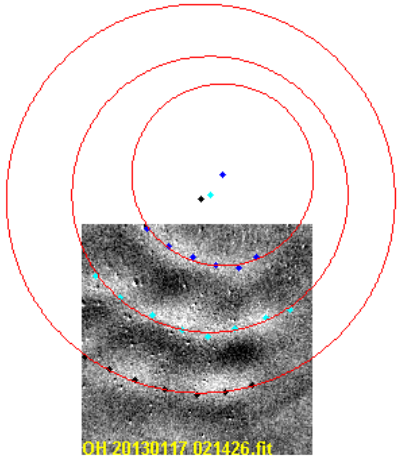

Figure 4.15: Airglow image with fitted circles and their epicentre at 16.jan 2013

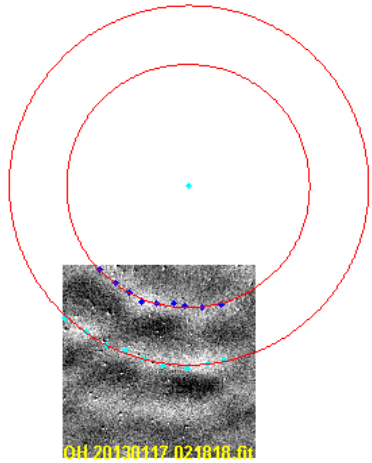

Figure 4.16: Airglow image with fitted circles and their epicentre at 16.jan 2013

Table 4.4: Geographic location of the observed gravity waves

Distance (km)	Angle (deg)	Direction of angle
65	56	west of south
51	47	west of south
34	25	west of south
77	56	west of south
77	53	west of south
55	46	west of south
70	29	south of west
71	33	south of west
65	54	west of south
71	27	south of west
62	31	south of west
60	55	west of south
91	26	south of west
92	26	south of west

CHAPTER 5
DISCUSSION

5.1 GROGRAT Ray-Tracing Results

Eleven different waves were run in GROGRAT. Out of these waves, nine propagated to the airglow region from heights in the lower atmosphere (troposphere and lower stratosphere), and two of the waves were evanescent, waves that do not propagate, according to GROGRAT.

The general tendency among the propagating waves suggest that the vast majority of the waves observed in the Trondheim wintertime OH nightglow are being generated in inland Norway, right in the mountainous part of Norway. These waves are generated in the troposphere or tropopause, the height varying from $\sim$ 4 km to just under 20 km, see table 4.1. Figure 4.2 shows that the bulk of the waves observed in the airglow have phase-speeds between 30 and 40 m/s. This would indicate that they are caused by airflow over the mountains launching freely propagating waves, i.e. waves propagating away from the source and not locked to the mountains themselves. A different type of mountain waves is *stationary*. In some cases, topographic forcing causes stationary waves to be formed. These waves have zero or close to zero horizontal phase speed [Schoeberl, 1985]. Such waves can be be observed in the OH ariglow images from certain nights; they are easy to spot in the airglow videos as wave structures that are not moving from frame to frame.

GROGRAT traced two of the waves' sources to locations just a little further out the Trondheimsfjord, and another wave propagated all the way from the south-west of Sweden, also from a source that is relatively close to the ocean. In addition, the mountain range Trollheimen, where another three waves were traced to, is also fairly close to the west-coast of Norway. This climate in this region is dominated by weather fronts coming in from the ocean in the west, often carrying moisture that is deposited as precipitation either in the form of rain in the summer season or snow in the winter season. It is therefore

unsurprising that the GROGRAT findings indicate high gravity wave activity in this area.

The lone wave source in southern Sweden is most likely also the result of weather fronts coming in over the land from the ocean. The close proximity to the coast means weather fronts coming in, depositing its moisture in the form of precipitation, and generally windy conditions.

A few of the other wave sources were located further inland, closer to the Swedish border. This is on the east side of the Norwegian mountain ridge. The climate conditions here are less windy and drier than those in the coastal areas. Topographic launching is the most likely candidate for generating these waves, as these sources are located on the lee side of the mountain range from airflow from the west.

A few of the waves are traced back to sources nearer to the coast than the mountains. Norwegian weather is generally unstable, with cold fronts regularly coming in from polar regions. The polar front forms where the cold, dry air from the Arctic region meets the warm, humid air from the south. The polar front flows in over Norway from west or south west all year, but is at its strongest in autumn/winter. The polar front is responsible for much of the precipitation in western Norway, along with orographic precipitation.

The constant presence of the polar front makes *frontogenesis* a possible candidate for generating large scale gravity wave activity in Norway. The tracing however, did not trace any waves to sources far off the western coast. Which is not to say that such wave sources do not exist; The direction of the waves might be wrong or filtering effects may be responsible for the waves not propagating to airglow layer heights.

It is worth noting that the waves processed in this thesis do not represent the full spectrum of gravity waves in the OH nightglow over Trondheim; waves were selected for processing based on criteria such as how clear the structures showed up against the night-sky background, how stable it appeared, and whether there was little to disturb the wave as it propagated.

Thunderstorms are rare at best in Norway, particularly in the winter season. Thus, thunderstorms are unlikely to be the source of the observed gravity waves. Seeing as convective activity in the tropics is thought to be responsible for the majority of global large scale gravity wave activity, there was a possibility that such waves could have travelled here from lower latitudes. Again, the absence of such sources in these results does not rule out the possibility of there being waves generated by convective activity at lower latitudes, but it is probably not the major source of momentum flux from the lower atmosphere into the MLT in this area.

All waves have sources located in the lower stratosphere or troposphere/tropopause. Consequently, auroral activity can probably be ruled out as the the source of the waves.

There is little zonal variation in the gravity wave locations; the sources are all found between 9.5° and 12.5° east. Further examination reveals that most of the wave sources are in fact east of Trondheim. This could be indicative of filtering at critical levels of eastward propagating gravity waves, possibly due to the zonal wind conditions in the area.

The weakness of the ray-tracing is the great temporal sensitivity of the HWM93. Because of very strong tides at Trondheim latitudes, the background winds changes very rapidly, see figure 3.10. This means that during the time it takes from the when the wave first appear in the OH nightglow images to it disappears from the images (often $\sim$ 30 min), the background winds may have changed enough that the wave goes from being a propagating wave to an evanescent wave according to GROGRAT.

5.2 Results from Geometric Localisation

Very few of the waves observed in the OH nightglow have curved wavefronts; for the most part the waves have wavefronts that at least *appear* straight. The limited field of view is responsible for this. It might be that several of the waves whose wavefronts look straight are in fact curved, but with such a large radius of curvature that in the limited field of view the wavefronts look straight. This limits the waves that can be studied in this manner to waves with a small radius of curvature, i.e. waves whose source is located relatively near to the imager site (a few hundred kilometres) compared to the ray tracer which is only limited by the input data and the background fields.

Using GROGRAT on the waves with circular wavefronts carries a certain risk, as GROGRAT assumes straight wavefronts. In addition, the curved wavefronts complicates the process, since it becomes much harder to find the direction of propagation of the waves. Still, the three waves whose wavefront displays a distinct curvature have been analysed with GROGRAT.

The gravity wave on December 3 2012, from 18:20 UTC and out, has its epicentre located about 150 km north west of the imager site, ($\sim$ 25° west of north). According to GROGRAT this wave is evanescent.

The gravity waves on January 16th have an epicentre estimated at about 150 km south west of Trondheim. This wave is not evanescent, and GROGRAT traces this wave to the coordinates (61.04°, 11.62°) and an altitude of 18.25 km. There is great discourse between the results of the two methods, both in direction and distance.

The gravity waves on January 17th from $\sim$ 02:00 UTC and on, have an epicentre located about 60 km south-west of the imager site. This wave is also evanescent according to GROGRAT.

Because of the low number of curved-wavefront gravity waves in the airglow images, it is impossible to say anything conclusive about the nature of these waves. There is a distinct possibility that the two waves that are found to be evanescent according to the ray-tracing scheme are in fact secondary waves, possibly the remnants of another wave originating in the lower atmosphere and propagating upwards until it breaks down in the mesosphere. Another possibility is that a gravity wave is being reflected off a critical layer. There is no evidence of the gridded pattern that one would expect for such a case. However, if the "wave train" happens to be only a few wavelengths long, and the angle of reflectance is right, the gridded pattern could be avoided. Particularly the wave on January 17 has such a small radius that if the source of the wave is located in the lower atmosphere, the angle of propagation would be very high.

The results from December 3 2012 differ significantly between the two different methods, both with respect to the direction and distance. However, the circle-fitting method has no way to incorporate diffraction effects in the model. Diffraction can be caused by wind fields or temperature and pressure gradients in the atmosphere.

CHAPTER 6
CONCLUSION

An all-sky camera system with a 45° field of view was set up at Dragvoll, Trondheim in the autumn of 2012. OH nightglow images were recorded during the winter season of 2012/2013. Two methods were applied to find the point of origin for the gravity waves; ray-tracing with GROGRAT and geometric localisation by fitting circles to the curvature of the curved-wavefronts gravity waves.

It was found that the majority of the observed gravity waves propagated from sources located along the Norwegian mountain ridge. This area seems to be responsible for generating the bulk of the gravity waves propagating into mesospheric regions over Trondheim. Topographic launching by airflow over mountains is considered to be the most likely candidate for generating these gravity waves.

This is not to say that the mountain ridge is the only gravity wave source. There were plenty of waves in the airglow images that were too unstable or had too irregularly shaped wavefronts for analysis of this kind. Furthermore, it is very likely that waves are being generated in the lower atmosphere that would be filtered out by the background winds at critical layers. Thus, they do not even reach the height of the OH airglow layer and cannot be observed in the nighglow images.

Only very few of the gravity waves had fronts with a distinct curvature. It might be that many of the waves whose fronts look straight are in fact curved, but the radius of curvature is too large for it to be discernible in the limited field of view. The data results from the ray-tracing and the circle-fitting method were in disagreement. Consequently, there must be diffraction phenomena in the atmosphere which the circle-fitting procedure fails to take into account.

CHAPTER 7

SUGGESTIONS FOR FUTURE WORK

In future, a similar project may use a different wind model, ideally one that has real-time wind data at mesospheric heights. The focus of this project should be on the ray-tracing procedure, as the circle-fitting method has proven to be unsuited to the imager's somewhat limited field of view.

Contrary to what is common procedure for GROGRAT ray-tracing, this project traced the waves down to the source from the region of observation. For future work, it would be interesting to trace waves from the area where majority of the waves have their geographic origin. A range of phase speeds and wavelengths should then be chosen to see which ones propagate into the OH airglow layer. Finally, a search should be performed for waves in the airglow images with the right characteristics. This would provide good insight into the diffraction and filtering processes that take place. Different wind models could be utilised and the results compared.

BIBLIOGRAPHY

Angelis, S. D., McNutt, S. R., Webley, P. W., 2011. Evidence of atmospheric gravity waves during the 2008 eruption of okmok volcano from seismic and remote sensing observations. Geophysical Research Letters 38 (10), 1159.

Dewan, E. M., Picard, R. H., 1998. Mesospheric bores. Journal of Geophysical Research 103 (D6), 6295–6305.

Dewan, E. M., Picard, R. H., 2001. On the origin of mesospheric bores. Journal of Geophysical Research 106 (D3), 2921–2927.

Dewan, E. M., Picard, R. H., O'Neil, R. R., Gardiner, H. A., Gibson, J., Mill, J. D., Richards, E., Kendra, M., Gallery, W. O., 1998. Msx satellite observations of thunderstorm-generated gravity waves in mid-wave infrared images of the upper stratosphere. Geophysical Research Letters 25 (7), 939–942.

Dörnbrack, A., Birner, T., Fix, A., Flentje, H., Meister, A., Schmid, H., Browell, E. V., Mahoney, M. J., 2002. Evidence for inertia gravity waves forming polar stratospheric clouds over scandinavia. Journal of Geophysical Research 107 (D20), SOL 30–1–SOL 30–18.

Durran, D. R., 1990. Mountain waves and downslope winds. Meteorological Monographs 23 (45), 59–83.

Geerts, B., Linacre, E., Nov. 1997. The height of the tropopause.
URL `http://www-das.uwyo.edu/~geerts/cwx/notes/chap01/tropo.html`

Hedin, A. E., 1991. Extension of the msis thermospheric model into the middle and lower atmosphere. Journal of Geophysical Research 96 (A2), 1159–1172.

Hedin, A. E., Fleming, E. L., Manson, A. H., Schmidlin, F. J., Avery, S. K., Clark, R. R., Franke, S. J., Fraser, G. J., Tsuda, T., Vial, F., Vincent, R. A., 1996. Empirical wind

model for the upper, middle and lower atmosphere. Journal of Atmospheric and Terrestrial Physics 58 (13), 1421–1447.

Lane, T. P. M., Reeder, J., Clark, T. L., 2001. Numerical modeling of gravity wave generation by deep tropical convection. Journal of Atmospheric Sciences 58, 1249–1274.

Lawrence, A. R., 2002. Observation of vertically-propagating atmospheric waves above antarctica. Ph.D. thesis, Darwin College, Cambridge.

Matsuno, T., 1971. A dynamical model of the stratospheric sudden warming. Journal of the Atmospheric Sciences 28, 1479–1494.

Nielsen, K., Taylor, M. J., Hibbins, R. E., Jarvis, M. J., 2009. Climatology of short-period mesospheric gravity waves over halley, antarctica (76°s, 27°w). Journal of Atmospheric and Solar-Terrestrial Physics 71, 991–1000.

P.Espy, 2012. personal communication.

P.Espy, 2013. personal communication.

Plane, J. M. C., 2003. Atmospheric chemistry of meteoric metals. Chemical Reviews 103 (12), 4963–4984.

R.Hibbins, 2013. personal communication.

Schoeberl, M. R., 1985. The penetration of mountain waves into the middle atmosphere. Journal of Atmospheric Sciences 42 (24), 2856–2864.

Smith, S. M., Taylor, M. J., Swenson, G. R., She, C., 2003. A multidiagnostic investigation of the mesospheric bore phenomenon. JOURNAL OF GEOPHYSICAL RESEARCH 108 (A2), 1083.

Swenson, G. R., Alexander, M. J., Haque, R., 2000. Dispersion imposed limits on atmospheric gravity waves in the mesosphere: Observations from oh airglow. Geophysical Research Letters 27 (6), 875–878.

Swenson, G. R., Liu, A. Z., 1998. A model for calculating acoustic gravity wave energy and momentum flux in the mesosphere from oh airglow. Geophysical Research Letters 25 (4), 477–480.

Taylor, M. J., Hapgood, M. A., 1988. Identification of a thunderstorm as a source of short period gravity waves in the upper atmosphere nightglow emission. Planer. Space Sci 36 (IO), 979–985.

TESTUD, J., 1970. Gravity waves generated during magnetic substorm. Journal of Atmospheric and Terrestrial Physics 32 (11), 1793–1805.

Vadas, S. L., Fritts, D. C., 2004. Thermospheric responses to gravity waves arising from mesoscale convective complexes. Journal of Atmospheric and Solar-Terrestrial Physics 66, 781– 804.

W.K.Hocking, 2001. personal communication.